Environmental and Climate Technologies
2024, vol. 28, no. 1, pp. 258–268
https://doi.org/10.2478/rtuect-2024-0021
https://content.sciendo.com

Designing a Fertilizing Robot Application Considering Energy Efficiency

Jüri OLT[1*], Olga LIIVAPUU[2], Indrek VIRRO[3], Tormi LILLERAND[4]

[1–4]*Estonian University of Life Sciences, Fr. R. Kreutzwaldi 56, 51006, Tartu, Estonia*

Received 01.04.2024; accepted 24.05.2024

***Abstract* – Electrically driven agricultural robots encounter accelerated battery depletion compared to vehicles operating on asphalt due to heightened rolling and traction resistance necessitating increased energy consumption. This issue becomes pronounced in regions devoid of access to the electrical grid, precluding the possibility of recharging electrically driven agricultural robots and consequently leading to interruptions in their uninterrupted functionality. To address this challenge, the agrorobotics working group at the Estonian University of Life Sciences devised a novel solution: a combined energy production station leveraging biogas, hydrogen, and solar energy. This station was integrated with a prototype autonomous fertilizing robot tailored for blueberry plantations to conduct precision fertilization on depleted milled peat fields. Distinctive features of the station encompass an automated battery exchange system and an electric generator equipped with a membrane motor. These components, in conjunction with a solar energy and electric generator control system, alongside a battery charger, are affixed onto a mobile platform. The primary objective of this study was to ascertain the energy requisites of an autonomous fertilizing robot during field traversal and while executing technological operations. To achieve this aim, the mechanical power and energy necessary for the operation of the robot fertilizer spreader were initially quantified. Subsequently, an accumulator possessing suitable power and capacity for the operation of the robot fertilizer spreader was chosen. The article further delineates the determination of the travel distance achievable by the robot on a single charge of the selected accumulator, in addition to evaluating the traction power efficiency and specific power.**

***Keywords* – Agricultural robots; berry plantation; energy consumption; power; precision fertilization.**

1. INTRODUCTION

Agricultural robots have been in development since the last century [1]. However, as per the analysis outlined in article [2], their particularly rapid development began around 2006. Since then, there has been a steady increase in the number of patent registrations and scientific articles on the subject. With the growing use of unmanned ground vehicles (UGV) and robots in agricultural production, the necessity for their servicing has become apparent [3]–[8].

If UGVs and robots are equipped with electric drives, they require electricity to operate. The batteries powering these machines become discharged during operation, necessitating the replacement of depleted batteries with charged ones to avoid work interruptions. However, agricultural production units, particularly fields, are often located far from residential areas

* Corresponding author.
E-mail address: jyri.olt@emu.ee

©2024 Author(s). This is an open access article licensed under the Creative Commons Attribution License (http://creativecommons.org/licenses/by/4.0).

and power grids. Therefore, the development of local mobile energy or power plants becomes a practical solution [9].

The energy consumption of the farming robot serves as the basis for determining the size or power of a local mobile power plant. This allows for the planning of electricity production and consumption flows [10]–[12]. Hence, determining the energy consumption of the farming robot is essential.

In the selection of an appropriate automated drive for agricultural robot, various technical, operational, and economic factors necessitate consideration [12]–[13]. Paramount among these considerations is the imperative that the chosen drive facilitates a seamless technological process, maintains predetermined productivity levels, and exhibits favourable economic performance. From various potential solutions, the most economically advantageous option must be chosen. The characteristics of the machinery and its drive are conceptualized as a comprehensive set, encapsulating all facets of the production process and the machinery's operation. These characteristics encompass technological, kinematic, energetic, mechanical, load, and inertia parameters. Technological parameters are elucidated through the presentation of a technological scheme, delineating the sequence of operational and idle cycles undertaken by the machinery. Specific energy consumption and productivity of the agricultural robot, contingent upon velocity, are derived from this technological process [14]. These characteristic values serve as the foundation for deriving other pertinent drive characteristics. Kinematic quantities are elucidated through kinematic diagrams, presenting the characteristics and sequence of transmissions between the robot's electric motor and its implements. Energetic parameters characterize power distribution among individual nodes of the machinery, thereby informing decisions regarding the energy requirements of these nodes and the overall machinery. Load diagrams show the dependence of moment, force or power on time or on the path travelled by the working body. A technological or kinematic process determines the change in these parameters. Inertial characteristic values denote the magnitude of the machinery's moment of inertia and the dynamics of its change, encompassing dynamic forces and moments. The physical dimensions of the drive and the design of the machinery wield substantial influence over drive selection. The initiation of electric drive design commences with a technical task, crafted in collaboration with technologists and production engineers. This task delineates the characteristic dimensions of the drive, operational conditions, safety protocols, and requisite work protection measures. Static moment variations, the necessity for speed regulation, starting and braking conditions, production operation sequences, automation requirements, environmental conditions, and energy supply status are integral components of the technical task. Given the interconnected nature of these design considerations, drive design is a collaborative endeavour, lacking a rigidly predefined sequence.

In the initial phase of the design process, the speed regulation mechanism for the drive is determined. If there is a need to adjust the drive speed, determinations regarding the drive type and current rating are made simultaneously. Drives prove to be cost-effective only when the duration of low-speed operation is minimized. Subsequently, in the second stage of design, the power rating of the specified motor type is selected. This entails the composition of a load diagram for the agricultural robot. Based on this analysis, the final motor power is determined, factoring in considerations of thermal stability and overload capacity. Concurrently, the appropriate rated motor rotation frequency is selected. In situations requiring frequent starts and reversals, preference is given to a motor with a rotational frequency that results in the shortest transient durations. In the subsequent phase of design, the control scheme for the drive is formulated, aligning with previously established overarching principles. In addition to fundamental aspects of drive operation such as starting,

braking, and speed regulation, measures to safeguard the drive and the machinery from abnormal conditions must be contemplated. Issues such as remote control, signalling, and technological oversight are addressed within this phase. Main and control circuits, as well as regulating and starting rheostats, are determined at this stage. The selection of starting device construction methodology should be contingent upon surrounding environmental conditions.

In the development of unmanned ground vehicles and agricultural robots, one must consider the purpose and required energy/power, or energy balance. For example, in planning the acquisition of electrical energy for conducting the technological process in a blueberry plantation established on depleted peat fields, it is necessary to clarify its volume, or to compile an electricity balance [15]. In this regard, the required power demand must first be determined.

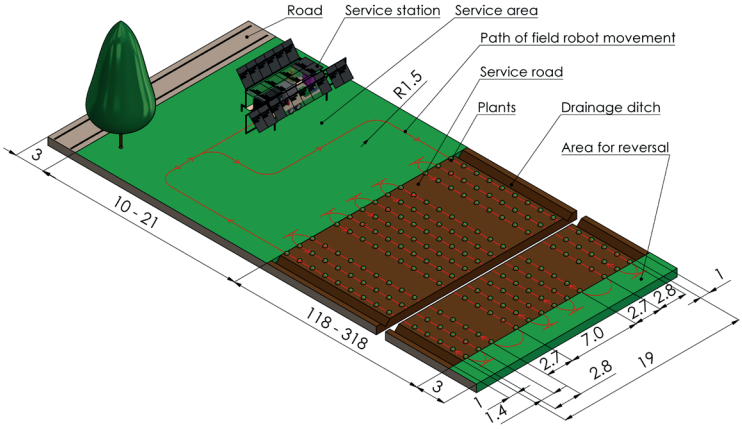

Fig. 1. Fragment of a field.

The aim of the research was to develop a methodology for calculating the tractive performance of an agricultural robot, ensuring its mobility over the unprepared peat terrain. It allows to determine the energy consumption of an agricultural robot during movement in the field (travel distance) and for performing technological operations (fertilizer distribution – delivering the prescribed amount of fertilizer to the right location) in blueberry plantations established on depleted peat fields (Fig. 1). Furthermore, the study aimed to select a suitable battery with appropriate parameters and optimize the parameters of technological tools, including the volume or fill level of the fertilizer hopper.

2. Power Distribution and Operational Dynamics of a Fertilizer Robot

The tractive performance justification of a fertilizer robot is important as it ensures the vehicle mobility across the depleted milled peat fields.

The total power of the fertilizer robot P_{total} includes three components: in addition to the power for movement, it also encompasses the power required for operating technological devices.

$$P_{\text{total}} = P_{\text{w}} + P_{\text{m}} + P_{\text{d}}, \tag{1}$$

where

P_w power for robot's movement, W;
P_m power required for operating the manipulator, W;
P_d power required for operating the dispenser, W.

When moving, the wheel of fertilizer robot rotates with a constant angular velocity and this angular speed is proportional to the engine rotation speed, depending on the gearing ratio in the drive train. The power transferred to the wheel axle P_w can be calculated as [16]:

$$P_w = T\omega \tag{2}$$

where
T torque transferred to the wheel axle, $T = F_k r_k$, N·m;
ω angular velocity of the wheel, rad·s^{-1};
F_k net tractive force, N;
r_k wheel rolling radius, m.

The theoretical velocity of the wheel is determined by the wheel's rotational velocity times the rolling radius $v_t = \omega r_k$, but the actual wheel velocity v_a is less due to the relative motion at the interface between the wheel and the surface. This relative motion is the travel reduction ratio or slip, and is defined as the ratio of the loss of wheel velocity to the theoretical velocity: $\delta = (v_t - v_a)/v_t$.

The value of the tangential tractive force generated by a wheel of the agricultural robot, depends on the applied normal load, the parameters of the wheel itself, the physical and mechanical properties of the ground surface, and the mode of movement (including the coefficient of slippage) and can be described as a function [17]:

$$F_k = f(\delta, f_k, G_w, k_o, r_o, b_o, \ldots) \tag{3}$$

where
δ slip coefficient of the robot's chassis;
f_k rolling resistance coefficient of the wheel;
G_w vertical operational load applied to the wheel, N;
k_o coefficient of volume compression of the ground surface;
r_o wheel static radius, m;
b_o wheel static width, m.

The rolling radius of the wheel r_k can be described in terms of its static radius r_o and the normal sag of its tire h_z:

$$r_k = r_o + h_z, \tag{4}$$

where tire deflection can be determined using the following relationship [17]:

$$h_z = \frac{G_w}{\pi \rho_w \sqrt{2 r_0 b_0}}, \tag{5}$$

where ρ_w is the air pressure inside the tire, Pa.

During the experimental investigations, the net tractive force F_k exerted by the drive wheels of the fertilizer robot includes two components: the drawbar pull and the rolling resistance [16]:

$$F_k = F_h + F_f. \tag{6}$$

The maximum tractive force exerted by the agricultural robot's wheel can represented by the following equation:

$$F_{\mathrm{kmax}} = \delta_{\max} \cdot A_{\mathrm{k}} \cdot k_{\mathrm{o}} \cdot L, \tag{7}$$

where

A_{k} sum of vertical projections of the tread lug surfaces plunged into the ground, m^2;
L length of the ground surface adhesive arch, m.

The contact length of the tire L can be computed by considering the vertical equilibrium of the tire [17]:

$$L = r_{\mathrm{k}} \left(\tan^{-1} \frac{f_{\mathrm{k}} \sqrt{1 - f_{\mathrm{k}}^2}}{\frac{1}{2} - f_{\mathrm{k}}^2} + 2 f_{\mathrm{k}}^2 \right) \tag{8}$$

The total sum of the vertical projections of the tread lug surfaces that penetrate into the ground on the wheel of the robot is calculated using the following equation [18]:

$$A_{\mathrm{k}} = \pi \cdot h_z \sqrt{(2r_0 - h_z) \cdot (b_0 - h_z)} \tag{9}$$

Simultaneously, the robot's ability to exert tractive power is contingent upon its adhesive properties. Consequently, it is important that the adhesive capability of the robot's wheel is adequate to produce the maximum tractive force: $F_{\mathrm{kmax}} = \mu G_{\mathrm{w}}$, where μ is the factor of traction for the robot's wheel interacting with the ground surface. It enables the computation of the maximum slip using the following formula:

$$\delta_{\max} = \frac{\mu \cdot G_{\mathrm{w}}}{\pi \cdot h_z \sqrt{(2r_0 - h_z) \cdot (b_0 - h_z)} \cdot k_0 (r_0 + h_z) \left(\tan^{-1} \frac{f_{\mathrm{k}} \sqrt{1 - f_{\mathrm{k}}^2}}{\frac{1}{2} - f_{\mathrm{k}}^2} + 2 f_{\mathrm{k}}^2 \right)} \tag{10}$$

Experimentally, the actual value of the wheel slip can be also determined as follows [19]:

$$\delta = 1 - \frac{n_{\mathrm{ko}}}{n_{\mathrm{km}}} \cdot \frac{v_{\mathrm{m}}}{v_0}, \tag{11}$$

where n_{ko} and n_{km} corresponding to the number of revolutions of the wheel over one and the same track distance to idle and working modes; v_{o} and v_{m} robot movement speeds corresponding to idle and working modes.

The weight of the fertilizer robot consists of two components - the empty weight of the fertilizer robot and the amount of fertilizer in the fertilizer hopper. A peculiarity of the fertilizer robot is that the second component constantly changes during operation; more specifically, it decreases with each fertilizer dose depending on the fertilization norm, so

$$G_{\mathrm{rob}} = m_{\mathrm{rob}} \cdot g = (m_{\mathrm{net}} + m_{\mathrm{f}} - n_{\mathrm{f}} \cdot q_{\mathrm{f}}) \cdot g, \tag{12}$$

where

m_{rob} total mass of the fertilizing robot; m_{net} mass of empty robot; m_{f} mass of fertilizer; n_{f} number of plants; q_{f} fertilization rate; g gravitational acceleration.

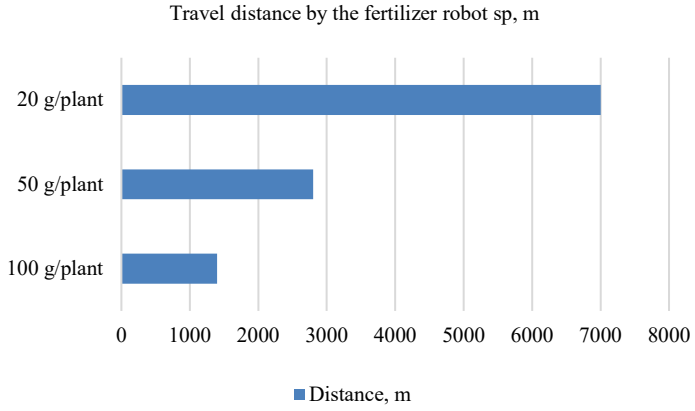

Fig. 2. Fragment distance travelled by the fertilizer robot in the blueberry field depends on the fertilization rate q_f.

Since the total fertilizer in the fertilizer hopper is distributed among the plants in the field or orchard, then

$$m_f = n_f \cdot q_f. \tag{13}$$

The distance between blueberry plants in a row varies greatly 0.915…1.8 m [20]. Taking the average distance between plants $l_p \approx 1.4$ m, then the distance covered by the fertilizer robot with the fertilizer in the hopper can be calculated as follows

$$s_p = n_f \cdot l_p. \tag{14}$$

Since the fertilization rate q_f = 20–100 g/plant, then the distance travelled by the fertilizer robot with one maximum amount of fertilizer in the hopper, whose mass m_f = 100 kg, ranges from 1.4 to 7.0 km (Fig. 2).

One working cycle consists of the fertilizer robot's technological movement from the service station to the plants, fertilization on the work track, movement from the work track to the service station, and the time spent on technological maintenance.

The average speed of the fertilizer robot's operational movement during fertilization (triangular movement cycle) is expressed as

$$v_{m.o} = \frac{s_p}{t_m} = \frac{s_a + s_d}{t_a + t_d + t_{s.1} + t_{s.2}}, \tag{15}$$

where

s_p path length of one movement of the fertilizer robot, or the distance between plants, where $s_p \neq$ const;
s_a distance of accelerating movement;
s_d braking distance;
t_m time taken to complete the entire movement cycle on the work track;
t_a time taken for accelerating movement;
t_d time taken for braking;
$t_{s.1}$ time for fertilizer dosing;
$t_{s.2}$ time required for delivering fertilizer to the plant.

To ensure proper functionality, it is essential to adhere to the precise trajectory, thus necessitating movement organized with minimal error and an optimal route.

The average speed of the fertilizer robot $v_{m.t}$ during technological movement from work track to the maintenance station (trapezoidal movement cycle) and from the maintenance station to the plants is expressed as

$$v_{m.t} = \frac{s_o}{t_a + t_p + t_d}, \tag{16}$$

where

s_o distance between service station and plants, where $s_o \neq$ const;
t_p time taken for movement at a programmed speed;
t_a time taken for accelerating movement;
t_d time taken for braking.

We will now examine the physical and mechanical properties of the ground surface. Despite the importance, the comprehensive investigation into how the parameters concerning the wheels of an agricultural robot, in conjunction with the inherent physical and mechanical characteristics of the traversed terrain, influence slippage remains insufficiently explored. Experimental research confirms that agricultural robot wheels rolling along permanent artificial tracks experience reduced slippage, leading to increased tractive force. However, it is important to note that the technological agricultural robot is specifically designed to operate in plantations established on depleted milled peat fields. The coefficient of volume compression of the undrained peat terrain k_o is between 8–10 N·cm^{-3}. The traction characteristics of an agricultural robot operating on porous soil are contingent upon the soil's capacity to withstand the horizontal deformation induced by the tread lugs of its wheels.

TABLE 1. FERTILIZER ROBOT'S SPECIFICATIONS

Vehicle parameters	
Mass, kg	350
Volume of the hopper, l	100
Movement speed, km h^{-1}	up to 5
Battery	60 V, 94 Ah
Engine power, kW	1.2
Wheel statics radius, m	0.28
Wheel static width, m	0.254
Overall length, m	1.9
Overall width, m	1.3
Overall height, m	1.5
Tire pressure, kPa	60

The fertilizer robot moves at a low speed, rendering the force of air resistance negligible.

By utilizing formulas (8)–(11) alongside the technical specifications of the fertilizer robot (Table 1) we can determine the coefficient of rolling resistance of the wheel f_k moving on the depleted milled peat fields. This coefficient falls within the range 0.14–0.2 and the maximum tractive force that is generated by the robot's wheel to be 396 N.

3. Energy Consumption for Fertilizer Robot

The drive system of the fertilizing robot operates in dynamic mode, characterized by alternating starts and braking. Consequently, it is imperative to initially assess the energetics of transient processes. Subsequent to this evaluation, the determination of motor power ensues, necessitating the availability of a load diagram specific to the agricultural robot. Initially, the selection of motor power relies upon insights derived from this load diagram. Subsequently, a motor load diagram is constructed through a detailed analysis of the transient process. The final selection of engine power is informed by this analysis, taking into account considerations such as heating effects and overload capacity.

The appropriate rated load frequency of the motor [min^{-1}] must be carefully determined. In scenarios involving frequent starts and stops, preference is given to a motor with a rotational frequency characterized by the shortest transient durations. Additionally, when selecting the motor, attention must be paid to its construction suitability. Subsequently, the drive control scheme is formulated, considering the aforementioned general principles. In addition to addressing fundamental aspects of drive operation such as starting, braking, and speed regulation, measures for safeguarding the drive system and the fertilizing robot from various abnormal conditions must be considered. This includes addressing issues related to remote control, signalling, and technological oversight. The selection of starting devices should be tailored to suit the prevailing environmental conditions [21].

The mechanical energy requirement, E_m [W·s or N·m], necessary for operating the fertilizer robot can be found as follows:

$$E_\text{m} = \frac{P_\text{total} \cdot t_\text{t}}{\eta_\text{t}} \tag{17}$$

or

$$E_\text{m} = \frac{F_\text{k} \cdot s}{\eta_\text{t}}, \tag{18}$$

where

t_t time taken to complete the entire working cycle, s;
s total distance travelled by the fertilizer robot, m;
$\eta_\text{t} = 0.6$ efficiency of transmission.

The total distance travelled by the fertilizer robot on a single battery charge can be viewed as the product of the number of working cycles of the fertilizing robot, s_ws, and multiplication factor, n_m:

$$s = s_\text{ws} \cdot n_\text{m}. \tag{19}$$

This can also be interpreted as the working stroke of the fertilizer robot. In this context, a working stroke s_ws accounts for the complete movement of the fertilizer robot in pairs of syringes across the field, starting from the end near the service station to the turning point at the other end of the field, which constitutes the total length of the plant rows $s_\text{ws.t}$, the return movement $s_\text{ws.u}$, and the movement back towards the service station end, covering the total length of the plant rows again $s_\text{ws.b}$, expressed as:

$$s_{ws} = s_{ws.t} + s_{ws.u} + s_{ws.b}. \tag{20}$$

As field lengths and consequently the lengths of plant rows vary across different fields, the number of working strokes during operation may vary. It would be reasonable to organize work in such a way that the number of working strokes during operation is an integer multiple. This saves time spent on idle movements and increases efficiency. Thus, considering equations (13), (19), (20), and (21), the number of working strokes n_m can be determined from the following equation:

$$n_m \cdot \frac{s_a}{s_{ws}} = \frac{E_m \cdot \eta_t}{F_k \cdot s_{ws}}, \tag{21}$$

Eq. (20) indicates that the number of working strokes depends on the energy available in the battery, the traction force required for the fertilizer robot's movement, and the length of the working stroke.

The mechanical energy requirement E_m needed to operate the fertilizer robot must be covered by electrical energy E_{el} in the case of an electric drive:

$$E_{el} = I \cdot U \cdot t, \tag{22}$$

where

I current consumed, A;
U voltage, V;
t time spent for work, s.

The drive of the fertilizer robot receives electrical energy from the accumulator, where a significant parameter, the battery capacity C [Ah] can be determined as follows:

$$C = \frac{E_{el}}{U} \tag{23}$$

or

$$C = I_a \frac{t}{3600}, \tag{24}$$

where I_a is the average electrical current used by the electric drive, A.

The energy capacity of the fertilizer robot's accumulator is $C = 94$ Ah. The charging and discharging requirements for the accumulator in its operation are as follows:

1. The battery can discharge during operation up to 20 % of its energy capacity, $C_{20\%} = 18.8$ Ah.
2. The battery can be charged up to 90 % of its energy capacity during charging, $C_{90\%} = 84.6$ Ah.

Thus $C_{usable} = C_{90\%} - C_{20\%} = 84.6 - 18.8 = 65.8$ Ah.

From Eq. (21), we obtain the usable electrical energy E_{el} for a battery voltage $U = 60$ V: $E_{70\%} = 65.8 \cdot 60 = 3948$ Wh.

The estimated power obtained from the solar station during operational conditions is $P_{el} = 4000$ W. On average, the losses from inversion are 100 W, resulting in the maximum power reaching the battery charger being $P_{MPPT} = 3900$ W. At the maximum power obtained from the solar panels, under ideal conditions, the time required for a single charge of the battery is:

$$t = \frac{E_{70\%}}{P_{MPPT}} = \frac{3948}{3900} = 1.01 \text{ h}.$$

4. CONCLUSION

1. Justifying the tractive performance of agricultural robots is crucial, as it ensures their mobility over fields with low carrying capacity. The fertilizer robot prototype's suitability in terms of its tractive performance is analysed by considering the robot's weight, ground pressure distribution and slippage. The development of the mathematical model in this study shows that the physical and mechanical properties of the ground surface play a significant role in determining the traction capabilities of agricultural robots. A comprehensive understanding of these parameters is crucial for optimizing slip coefficients and tractive force. In the case of the fertilizer robot prototype driving on the field with a soil volume compression coefficient k_o = 10 N·cm^{-3}, a maximum tangential (tractive) force of 1584 N was identified, facilitating the calculation of the necessary power to propel the agricultural robot. It allows for determining the energy consumption of the fertilizer robot both during its movement in the blueberry field and while performing technological operations.
2. Energy storage and usage that is independent of location ensures access to critical services and machinery operation in rural areas. The goal of constructing the mobile power station is to provide energy for agricultural robot prototype in remote areas lacking an energy grid and infrastructure. Energy consumption analysis of the fertilizer robot revealed a dynamic operational mode characterized by alternating starts and stops. The primary energy source for the developed power station is photovoltaic panels generating 3900 W. The developed power station is equipped is autonomous charging and battery replacement stations. It was shown that, under ideal conditions, the time required for a single battery charge at maximum power from the solar panels is 1.01 hours.

ACKNOWLEDGEMENT

This research was supported by development fund PM210001TIBT from the Estonian University of Life Sciences and proof-of-concept grant EAG304 from the Estonian Research Council.

REFERENCES

[1] Li M., Imou K., Wakabayashi K., Yokoyama S. Review of research on agricultural vehicle autonomous guidance. *Int J Agric & Biol Eng* 2009:2(3).
[2] Zhao J., Yang Y., Zheng H., Dong Y. Global Agricultural Robotics Research and Development: Trend Forecasts. *Journal of Physics: Conference Series* 2020:1693:012227. https://doi.org/10.1088/1742-6596/1693/1/012227
[3] Hajjaj S. S. H., Sahari K. S. M. Review of Research in the Area of Agriculture. *Lecture Notes in Electrical Engineering*. Springer, Singapore 2014:291:107–117. https://doi.org/10.1007/978-981-4585-42-2_13
[4] Bechar A., Vigneault C. Agricultural robots for field operations: Concepts and components. *Biosystems Engineering* 2016:149:94–111. https://doi.org/10.1016/j.biosystemseng.2016.06.014
[5] Bechar A., Vigneault C. Agricultural robots for field operations: part 2: Operation and systems. *Biosystems Engineering* 2017:153:110–128. https://doi.org/10.1016/j.biosystemseng.2016.11.004
[6] Aravind K. R., Raja P., Perez-Ruiz M. Task-based agricultural mobile robots in arable farming: A review. *Spanish Journal of Agricultural Research* 2017:15(1):e02R01. https://doi.org/10.5424/sjar/2017151-9573
[7] Marinoudi V., Sørensen C. G., Pearson S., Bochtis D. Robotics and labour in agriculture. A context consideration. *Biosystems Engineering* 2019:184:111–121. https://doi.org/10.1016/j.biosystemseng.2019.06.013
[8] Kägo R., Vellak P., Ehrpais H., Noorma M., Olt J. Assessment of power characteristics of unmanned tractor for operations on peat fields. *Agronomy Research* 2022:20(2):261–274. https://doi.org/10.15159/AR.22.001

[9] Green O., Schmidt T., Pietrzkowski R. P., Jensen K., Larsen M., Nyholm Jørgensen R. H. A. Commercial Autonomous Agricultural Platform – Kongskilde Robotti. In: Proceedings of the Second International Conference on Robotics, Associated High-Technologies and Equipment for Agriculture and Forestry RHEA 2014. *New trends in mobile robotics, perception and actuation for agriculture and forestry* 2014:351–356.

[10] Mitkov I., Harizanov V., Komitov G. Determining the energy efficiency of an agrorobot. *Agricultural Sciences* 2021:13(30):73–78. https://doi.org/10.22620/agrisci.2021.30.010

[11] Valdmanis G., Rieksta M., Luksta I. Solar energy based charging for electric vehicles at fuel stations. *Environmental and Climate Technologies* 2022:26(1):1169–1181. https://doi.org/10.2478/rtuect-2022-0088

[12] Candra O., Chammam A., Rahardja U., Ramirez-Coronel A., Al-Jaleel A., Al-Kharsan I. H., Muda I., Derakhshani G., Rezai M. M. Optimal Participation of the Renewable Energy in Microgrids with Load Management Strategy. *Environmental and Climate Technologies* 2023:27(1):56–66. https://doi.org/10.2478/rtuect-2023-0005

[13] Abdel Hamid R. H., Elidrissi Y., Elsamahy A., Regragui M., Menoufi K. Examining the Impact of Different Technical and Environmental Parameters on the Performance of Photovoltaic Modules. *Environmental and Climate Technologies* 2023:27(1):56–66. https://doi.org/10.2478/rtuect-2021-0001

[14] Virro I., Arak M., Maksarov V., Olt J. Precision fertilisation technologies for berry plantation. *Agronomy Research* 2020:18(S4):2797–2810. https://doi.org/10.15159/AR.20.207

[15] Arak M., Olt J. Technological description for automating the cultivation of blueberries in blueberry plantations established on depleted peat milling fields. Proceedings of the 9th Int. Sci. Conference Rural Development. *Research and Innovation for Bioeconomy* 2019. https://doi.org/10.15544/RD.2019.024

[16] Queiroz D. M., Schuller J. K. Traction. In: Holden N. M., Wolfe M. L., Ogejo J. A., Cummins E. J. (Ed). *Introduction to Biosystems Engineering* 2020. https://doi.org/10.21061/IntroBiosystemsEngineering/Traction

[17] Bulgakov V., Olt J., Kuvachov V., Smolinsky S. A theoretical and experimental study of the traction properties of agricultural gantry systems. *Journal of Agricultural Science* 2020:31(1):10–16. https://doi.org/10.15159/jas.20.08

[18] Rahman A., Yahya A., Mohiuddin A. K. M. Tractive Performance of LGP-30 Wheeled Vehicle During Straight Motion on Sepang Peat Terrain in Malaysia. *The Open Transportation Journal* 2009:3(1):15–28. https://doi.org/10.2174/1874447800903010015

[19] Kurkauskas V., Janulevicius A., Pupinis G. Influence of inflation pressure in tires on traction ratio 2WD and 4WD driving modes of tractor. *Engineering of Rural Development* 2016:448–455.

[20] Arak M., Olt J. Technological description for automating the cultivation of blueberries in blueberry plantations established on depleted peat milling fields. Proceedings of the 9th Int. Sci. Conference Rural Development. *Research and Innovation for Bioeconomy* 2019:6. https://doi.org/10.15544/RD.2019.024

[21] Kacare M., Pakere I., Grāvelsiņš A., Blumberga D. Spatial Analysis of Renewable Energy Sources. *Environmental and Climate Technologies* 2021:25(1):865–878. https://doi.org/10.2478/rtuect-2021-0065